Noname manuscript No.
(will be inserted by the editor)

Real-time Single Scattering Inside Inhomogeneous Materials

D. Bernabei · F. Ganovelli · N. Pietroni · P. Cignoni · S. Pattanaik · R. Scopigno

the date of receipt and acceptance should be inserted later

Abstract In this paper we propose a novel technique to perform real-time rendering of translucent inhomogeneous materials, one of the most well known problems of Computer Graphics. The developed technique is based on an adaptive volumetric point sampling, done in a preprocessing stage, which associates to each sample the optical depth for a predefined set of directions. This information is then used by a rendering algorithm that combines the object's surface rasterization with a ray tracing algorithm, implemented on the graphics processor, to compose the final image. This approach allows us to simulate light scattering phenomena for inhomogeneous isotropic materials in real time with an arbitrary number of light sources. We tested our algorithm by comparing the produced images with the result of ray tracing and showed that the technique is effective.

1 Introduction

Realistic visualization is one of the most important goals in Computer Graphics research. Over the last twenty years, rendering engines have become capable of producing images that are nearly indistinguishable from real life photographs. These results, however, often come at the expense of hours of computations. In recent years, since the advent of cheap, powerful, and now ubiquitous, dedicated graphic devices, much attention has been devoted on replicating the same effects in real time on end-user machines. Although convincing renderings of objects have been produced using graphic devices, many complex lighting effects are still subject of intense study. In particular, various types of common materials, such as wax, marble, skin, just to name a few, exhibit peculiar lighting effects commonly known as subsurface scattering. In these materials,

D. Bernabei
ISTI-CNR, Italy – Univ. Central Florida, Usa
E-mail: danielebernabei@gmail.com

F. Ganovelli, N. Pietroni, P. Cignoni, R. Scopigno
ISTI - CNR, Italy E-mail: surname@isti.cnr.it

S. Pattanaik
Univ. Central Florida, Usa E-mail: sumant@cs.ucf.edu

in fact, the light is not only reflected by the surface of the object, but it partially penetrates underneath and changes direction multiple times before being absorbed or leaving the object. Reproducing these interactions in real-time is a challenging task. In fact, in order to determine the correct illumination of a surface point, it is necessary to determine all paths taken by photons under the surface, and evaluate how material properties attenuate light intensity along these paths.

Many models have been proposed to simplify scattering phenomena. One of these simplifications consists in separately studying lighting effects when either only one or an undetermined high number of scattering event is assumed to take place. Another common assumption is to consider materials as isotropic. This last assumption has allowed, in recent years, the derivation of analytical formulae that permit the computation of subsurface scattering without explicitly determining the path taken by light rays. However, if the material is assumed to be inhomogeneous, analytic formulations result impossible and precomputing certain quantities seems to be the only solution to achieve interactivity. Precomputation, on the other hand, requires that some object or scene attributes remain static during run-time, thus limiting the usefulness of the algorithms. For this reason, Computer Graphics research has striven to reduce the number of limitations imposed by precomputation techniques, and this work is no exception.

We propose a compact and efficient representation of inhomogeneous material properties in order to compute scattering effects at run time with a single pass algorithm. Our algorithm proceeds by sampling the volume and computing, for each sample, the exponential attenuation of light due to optical density and depth in a set of uniformly distributed directions. This information is stored within the sample using spherical harmonics compression and used at rendering time to compute the percentage of light scattered towards the viewer. The rendering consists of displaying the boundary of the object as a normal surface mesh accounting only for purely superficial effects and then adding the contribution of the volumetric sampling.
The contribution of this paper is twofold:

- An efficient, *single-pass* algorithm for real time rendering of single scattering effects which completely decouples scattering phenomena from superficial light reflection computations, and that can be well integrated in standard rendering pipelines.
- A strategy for an adaptive opacity-dependent point sampling of the volume enclosed by a surface that is able to capture and represent the internal appearance of the object.

The rest of the paper is structured as follows. In Section 2 we will review the current state of the art on methods for real time rendering of scattering phenomena, with particular attention to the methods that have mostly influenced our work. In Section 3 we will present our technique in detail, in Section 5 we will discuss some results obtained by applying our approach and then in Chapter 6 future directions for this work will be analyzed.

2 Related work

Although many offline methods has been developed to accurately render scattering phenomena [4], interactive or real-time methods developed so far still suffer from various limitations. In the context of offline rendering, the volume rendering equation has been often solved with Stochastic Monte Carlo methods or Numerical Simulations and

Finite element methods. Monte Carlo Methods [13,15,21,30] have slow convergence and despite many acceleration and precomputation techniques, they are still unusable for interactive rendering [17]. Radiosity methods and numerical simulation [8,18,26,27,31], which do not employ randomization, require instead the precomputation of an elevated number of factors, thus requiring a significant amount of space. Nonetheless, these methods do not achieve the speed needed for real-time rendering, although significant improvements have been brought by the advent of graphics hardware programmability [3].

2.1 Analytic Single Scattering Solutions

The quest for an analytic formulation of the single scattering problem can be dated back to Blinn [2]. Hanrahan and Krueger [9] derived analytic expressions for layered surfaces by using linear transport theory, while Narashiman and Nayar [24] found a formula for the scattering of isotropic lights in spherical mediums. More recently Venceslas et al. [1] found a more general polynomial approximation that yields plausible results. Sun et al. [32] built a method based on an explicit, exact, analytic solution of the single scattering integral for isotropic point lights in homogeneous participating media. Zhou et al. [37] relaxed the homogeneous material restriction, introducing Gaussian RBFs to model variations in material density, a common representation for sparse media like clouds [7,11]. A recent paper on Ray Marching by Zhou [36] follows his previous work in using Gaussian RBFs to define medium density but adds a high-resolution residual field to incorporate fine media details present in smoke.

2.2 Precomputation

Many of the presented approaches can be significantly speeded-up by precomputating some portion of the rendering process. Premože et al. [25] precomputed incoming light at every point in a scalar field and used the complex path integration mathematics to approximate forward scattering. Hegeman et al. [12] used the same mathematical framework incorporating the same ideas for volume rendering of translucent materials by Kniss et al. [19, 20]. In their seminal papers, Sloan et al. [28, 29] used a Spherical Harmonics basis to encode, for each vertex, a transfer function that maps incoming illumination to "transferred" radiance. By encoding distant, low frequency illumination in the same basis as the surface transfer function, surface rendering is reduced to a vector matrix-multiplication.

2.3 Dipole

The work by Stam [31] introduced the idea of modeling multiple subsurface scattering as a diffusion process. This model can be reasonably applied, to homogeneous materials only, because light distribution in highly scattering media tends to become isotropic. Jensen et al. [16] introduced a simplified model that, following such approximation, further simplifies light transport by using two virtual lights for each incoming ray. This method has been accelerated by smart precomputation techniques [10,14,22,23,34]. In particular, Dachsbacher and Stamminger [6], adapted the common shadow mapping

technique to use it with the dipole approximation, introducing the Translucent Shadow Maps.

An assumption commonly made by the existing approaches is that if an object is rigid than it is sufficient to model its boundary or at most adding a few internally layered surfaces, relying on the fact that the only significant scattering events happen just under the external surface. This is true most of the time but there are types of objects where the light interaction is dominated by scattering events well inside the volume, even if they have partially opaque surfaces. This is the case, for example, a jar of marmalade or a jellyfish. Walter et al. [33] proposed an algorithm for interactive rendering for the special case of objects enclosed in a refractive media, where deviation of lights entering the media plays the bigger role in the final image. Their method is based on a half-vector formulation of the problem which enable a fast iterative algorithm to find, for each point inside the volume and a light source, the points on the surface where the incoming rays are deviated to said point. Very recently Wang et al. [35] proposed a technique to interactively render translucent objects, by building a tetraehdralization of the volume in a preprocessing step and using the center of tetrahedra as nodes of a quad connected graph which is stored as a texture and used to solve the diffusion equation. Thanks to this parametrization, their algorithm also work, to some extent, also for deformable objects.

3 Rendering Single Scattering

Our approach consists of encoding the scattering properties of the object in a carefully chosen set of sampling points placed inside the volume, as shown in Figure 1. Each sample represents a small spherical region of volume for which it stores a direction-dependent optical depth function. At rendering time, the scattering term is integrated along each view ray by rendering the spheres and performing the integration in a fragment shader as in [37]. The substantial difference with their approach (and similar ones for participating media) is that, thanks to the precomputation of the optical depth, we do not need to do a rendering pass for each light in order to accumulate the irradiance on the samples.

3.1 Single Scattering from Directional Optical Depth.

Below we show how to approximate the volume rendering equation in terms of a set of sampling points and associated direction-dependent optical depth function.

Ignoring emissive materials, the volume rendering equation can be written as:

$$\nabla_{\boldsymbol{\omega}} L(x,\boldsymbol{\omega}) = \underbrace{-\sigma_t(x)L(x,\boldsymbol{\omega})}_{\text{extinction}} + \underbrace{\sigma_s(x)\int_{\boldsymbol{\xi}} p(\boldsymbol{\omega},\boldsymbol{\xi})L(x,\boldsymbol{\xi})\,d\Omega(\boldsymbol{\xi})}_{\text{in-scattering}} \tag{1}$$

where $L(x,\boldsymbol{\omega})$ is the radiance at point x towards direction $\boldsymbol{\omega}$, $\sigma_s(x)$ and $\sigma_t(x)$ are the scattering and extinction coefficients, respectively, and p is the phase function.

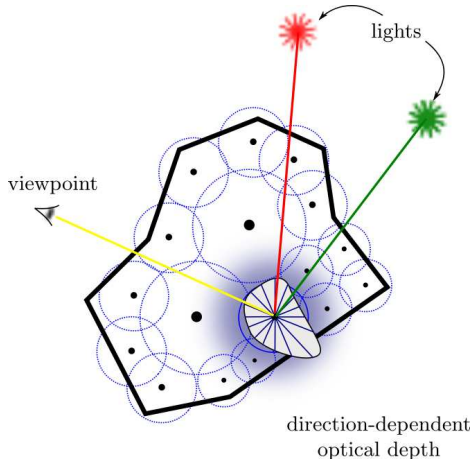

Fig. 1 An overview image of our algorithm: the direction-dependent optical depth is sampled and stored in a set of locations, and it is used at rendering to compute in a single pass the scattering of light.

The volumes with which we are dealing are defined by an enclosing surface S. Lights cannot be placed inside the volume; therefore, as surface points are the only receivers of direct, unattenuated lighting, we will treat them as the sole emitters of light (L_i) within the volume.

Solving the differential equation 1 for the unknown function $L(x, \boldsymbol{\omega})$, we obtain an equation in the form of an integral along a ray from x to y, two surface points along viewing direction $\boldsymbol{\omega}$.

$$L_{(ss)}(x, \boldsymbol{\omega}) = \underbrace{e^{-\hat{\tau}(x,-\boldsymbol{\omega})} F_t L_i(y, \boldsymbol{\omega})}_{\text{attenuated direct light}} + \underbrace{\int_x^y e^{-\hat{\tau}(x',\boldsymbol{\omega})} \sigma_s(x') \int_{\boldsymbol{\xi}} p(\boldsymbol{\omega}, \boldsymbol{\xi}) L(x', \boldsymbol{\xi})\, d\Omega(\boldsymbol{\xi})\, dx'}_{\text{in-scattered lighting}} \tag{2}$$

where

$$e^{-\hat{\tau}(x,-\boldsymbol{\omega})} = \tau(x, y) = \int_x^y \sigma_t(x')dx'$$

y being the first point of the surface encountered by a ray leaving from x towards direction $\boldsymbol{\omega}$.
The first term of equation 2 describes how surface point y, receiving light from outside the mesh, retransmits a certain quantity F_t, determined by Fresnel's law, towards direction $\boldsymbol{\omega}$ inside the volume. This attenuated direct lighting is a visible phenomenon only when the viewer is directly facing the light, and as we will limit the discussion from now on to point light sources, i.e. invisible sources, we will drop the first term of the above equation and concentrate on the second.

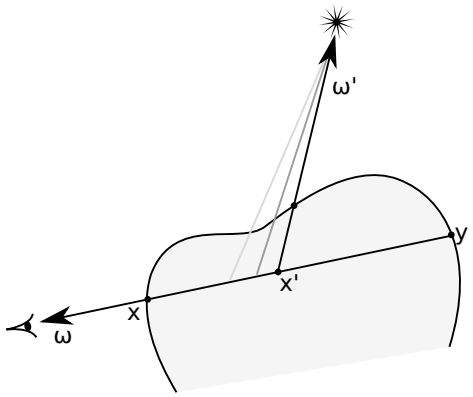

Fig. 2 Single Scattering of Light The contribution of single scattering of light at point x in direction $\boldsymbol{\omega}$ is computed by integrating, for each point x' along the ray from x to y, the attenuated amount of light received from direction $\boldsymbol{\xi}$ and retransmitted towards ω.

$$L_{(ss)}(x,\boldsymbol{\omega}) = \int_x^y \underbrace{e^{-\hat{\tau}(x',\boldsymbol{\omega})}}_{\text{attenuation factor}} \underbrace{\sigma_s(x')}_{\text{scattering}} \int_{\boldsymbol{\xi}} \underbrace{p(\boldsymbol{\omega},\boldsymbol{\xi})}_{\text{phase function}} \underbrace{L(x',\boldsymbol{\xi})}_{\text{incoming light}} \, d\Omega(\boldsymbol{\xi})\, dx'$$

In this equation, term $L(x',\boldsymbol{\xi})$ is still left unspecified. Light arriving at point x', located deeply inside the volume, could be recursively determined by the very same equation. But, if we assume that only one scattering event can occur, then $L(x',\boldsymbol{\xi})$ is only the attenuated direct lighting coming from the surface, therefore we set:

$$L(x',\boldsymbol{\xi}) = e^{-\hat{\tau}(x',\boldsymbol{\xi})} F_t L_i(x',\boldsymbol{\xi})$$

The total amount of light that exits at point x towards direction $\boldsymbol{\omega}$ is given by the sum of the reflected radiance and the scattered radiance, i.e.:

Radiance at point x towards $\boldsymbol{\omega}$ is therefore given by:

$$\underbrace{L_{(o)}(x,\boldsymbol{\omega})}_{\text{total outgoing light}} = \underbrace{L_{(ss)}(x,\boldsymbol{\omega})}_{\text{single scattered light}} + \underbrace{(1-F_t)L_{(r)}(x,\boldsymbol{\omega})}_{\text{reflected light}}$$

The term $L_{(r)}(x,\boldsymbol{\omega})$, in the context of our on-line rendering application, will be calculated using one of the popular shading models used by OpenGL.

For the sake of simplicity, we assume that scattering is isotropic, hence $p(\boldsymbol{\omega},\boldsymbol{\xi}) = k$; moreover, we will refer to the integrand function as $f(x')$,

$$L_{(ss)}(x,\boldsymbol{\omega}) = \int_x^y \underbrace{e^{-\hat{\tau}(x',\boldsymbol{\omega})}\sigma_s(x')k \int_{\boldsymbol{\xi}} L(x',\boldsymbol{\xi})\, d\Omega(\boldsymbol{\xi})}_{f(x')}\, dx'$$

We would like now to evaluate $f(x')$ only at discrete points within the volume and interpolate them when integrating along a ray. To this end, we will properly choose

a set of sampling points $B = \{b_i\}$ and associate to each sample a Gaussian radial basis function as in [37] $\Gamma = \{\gamma_i(x)\}$, where $\gamma_i(x) = e^{a_i||x-b_i||}$. Then we can use the following approximation:

$$\int_x^y f(x')\,dx' \approx \int_x^y f(x') \sum_i \gamma_i(x')\;dx' = \sum_i \int_x^y f(x')\gamma_i(x')\,dx'$$

It is intuitive that, if Gaussians have small radii of influence with respect to the dimensions of the surface, then $f(x')$, whose value strongly depends on the distance from the surface, will have little variance inside said radius. Therefore, we can assume $f(x')$ to be constant and take its value at point b_i.

$$\sum_i \int_x^y f(x')\gamma_i(x')\,dx \approx \sum_i f(b_i) \int_x^y \gamma_i(x')\,dx'$$

$$L_{(ss)}(x,\boldsymbol{\omega}) \approx \sum_{i\in\Gamma} \underbrace{k\sigma_s(b_i)e^{-\hat{\tau}(b_i,\boldsymbol{\omega})} \int_{\boldsymbol{\xi}} e^{-\hat{\tau}(b_i,\boldsymbol{\xi})} F_t L(b_i,\boldsymbol{\xi}) d\Omega(\boldsymbol{\xi})}_{f(b_i)} \int_x^y \gamma_i(x')\,dx'$$

By encoding the exponential attenuation due to the optical depth of each Gaussian center with Spherical Harmonics ψ_i, we can write down the formula used in our on-line computations:

$$L_{(ss)}(x,\boldsymbol{\omega}) \approx \sum_{i\in\Gamma} \underbrace{k\sigma_s(b_i)\psi_i(\boldsymbol{\omega})}_{\text{constant per sample}} \underbrace{\int_{\boldsymbol{\xi}} \psi_i(\boldsymbol{\xi}) F_t L(b_i,\boldsymbol{\omega})\,d\Omega(\boldsymbol{\xi})}_{\text{function of lights}} \underbrace{\int_x^y \gamma_i(x')\,dx'}_{\text{function of view ray}} \tag{3}$$

This equation expresses the radiance exiting at point x towards direction $\boldsymbol{\omega}$ as a sum of three-term products where the first term is constant per sample, the second is a function of incoming light and the third is a function of the sole viewing ray. If the light is arriving only from a finite number of directions D, the first integral reduces to a sum of D terms where each term requires the evaluation of a spherical harmonic. If lighting is defined over the whole sphere of directions, like when environment maps are used, then by projecting it over the Spherical Harmonics basis the above integral will reduce to a simple dot product of two vectors of coefficients.

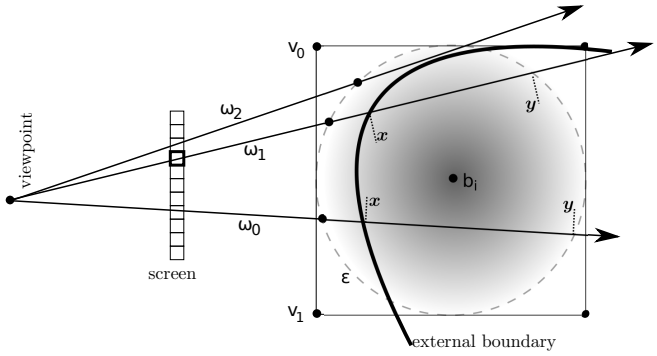

Fig. 3 Rendering Integration along the viewing ray and clipping against the external boundary of the object.

3.2 Rendering algorithm

The rendering algorithm consists of two steps. In the first step the input mesh is rendered, according to a simple surface lighting model (in our tests we used Phong lighting and shading but others are seamless integrable). The depth buffer produced by the rendering is then used to clip the region covered by the radial basis functions of the volume sampling points.

In the second step the term $L_{(ss)}(x, \boldsymbol{\omega})$ of equation 3 is computed by rasterizing all the balls corresponding to the samples and thus activating the fragment shaders that perform the necessary computation for each ray. Figure 3 shows a scheme with a single sphere and three rays. For each ray the fragment program evaluates the integral $\int_x^y \gamma_i(x')\, dx'$ in the equation 3 between x and y, where x is the maximum between the depth value stored in the buffer for the fragment and the first intersection with the ball and y is the second intersection of the ray with the ball and as. Please notice that if $x > y$, as for the ray ω_2, it means the portion of ray inside the ball is outside the boundary and the corresponding contribution to the line integral is 0. The primary goal of the method is to avoid fuzzy borders by ensuring that the silohuette of the object is determined only by the mesh boundary. Figure 3 shows the difference between using or not clipping on a close up of the gargoyle model. It can be argued that his clipping is not done against the whole boundary but only against the part visible from the viewer, i.e. the line integral is performed also in those parts of ray exiting from the object but still inside some ball, but the effect on the final result is negligible.

4 Point Sampling Direction-Dependent Optical Depth.

The core of the preprocessing stage revolves around finding good positions for the samples inside the volume. The sampling algorithm is critical not only to minimize memory occupation and rendering time, but also to ensure that the assumptions made in our derivation are valid.

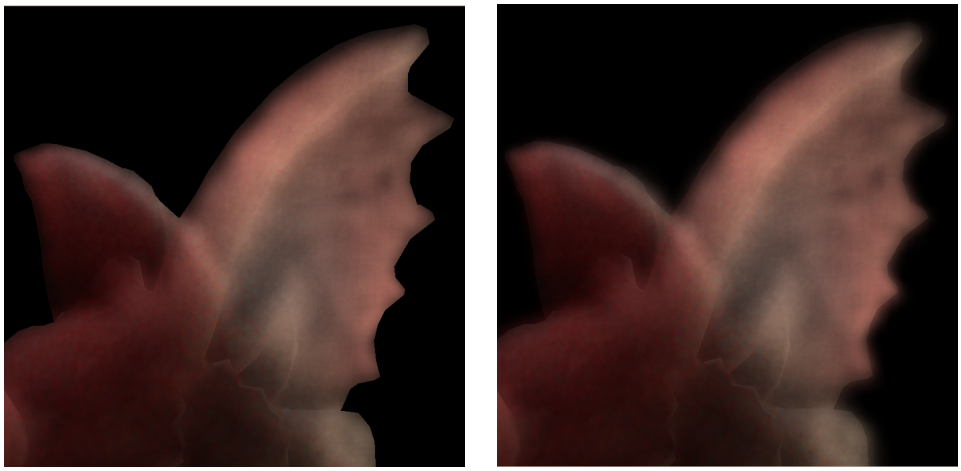

Fig. 4 Comparison of a close up of the Gargoyle model when clipping is used (left) or not used (right).

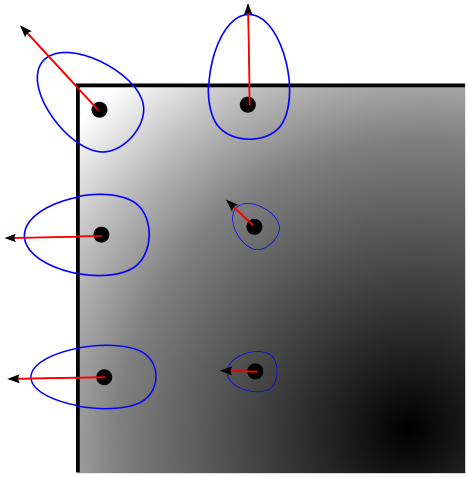

Fig. 5 For each point the shape of the direction-dependent optical depth and its first moment are shown (rendered with blue contours and red arrows, respectively). The gray level represent the divergence of this moment, which will be higher close to the corners and in general where the surface change abruptly.

4.1 A sound heuristic for sampling density

When sampling a scalar field, we can place the samples with a density dependent on the variation of the scalar field. In our case, the sampled value is the direction-dependent optical depth function $\psi_i(\boldsymbol{\omega}) = e^{-\hat{\tau}(b_i,\boldsymbol{\omega})}$. However, as shown below, we can derive a meaningful scalar value for the density of our sampling from the function ψ_i.

Since ψ_i decreases exponentially with the optical depth $\hat{\tau}(b_i, \boldsymbol{\omega})$, it follows that it will be strongly peaked at directions corresponding to minimal $\hat{\tau}(b_i, \boldsymbol{\omega})$, as exemplified

(a) (b) (c) (d)

Fig. 6 Steps of the sampling algorithm: a section of the volume. (a) original mesh boundary and density (the density is constant in this example) (b) optical depth for the direction orthogonal to the section (c) absolute value of the divergence $\rho(x) = |\nabla \cdot \mathbf{T}(x)|$ (d) final samples.

in Figure 5. In the limit case, the function $\psi_i(\boldsymbol{\omega})$ defined at a point x placed at an infinitesimal distance beneath the surface, will present an extreme peak in the same direction as the normal to the surface.
Since the function is strongly peaked, we can take its first moment as a reliable indicator of its shape and behavior:

$$\mathbf{T}(x) = \int e^{-\hat{\tau}(x,\boldsymbol{\omega})} \cdot \boldsymbol{\omega}\, d\Omega(\boldsymbol{\omega}) \tag{4}$$

Function $\mathbf{T}(x)$ defines a vector field whose values point towards the mean direction of minimum optical distance at each point. Moreover, the norm of these vectors, $||\mathbf{T}(x)||_2$ gives us a weighted mean of the attenuation factor over all directions. The sampling density needs to reflect changes in shape of $e^{-\hat{\tau}(x,\boldsymbol{\omega})}$ with respect to x, therefore the quantity that is more apt to estimate optimal density is the absolute value of the divergence of the aforementioned vector field. In fact, in areas where the principal direction of light changes rapidly, e.g. at corners, divergence will be higher; similarly in areas where the magnitude of the principal direction decreases rapidly, this value will be high as well, e.g. near the surface, exactly where we expect scattering phenomena to be more pronounced. Therefore we set the sampling density as: $\rho(x) = |\nabla \cdot \mathbf{T}(x)|$

4.2 Efficient sampling of direction-dependent optical depth

Now that we have the function $\rho(x)$ which tells us the sampling density we want to distribute samples accordingly and in a efficient manner. The sampling algorithm takes a watertight mesh and a regular sampling of the material density inside the mesh (Figure 6.(a)), and returns a set of samples and relative SPH compressed direction dependent optical depth (Figure 6.(d)). It consists of 5 steps, detailed in the following:

Compute Direction Dependent Optical Depth: $\psi_i(\boldsymbol{\omega})$
The optical depth is sampled for a fixed number n of directions, which is parameter of the algorihm. For each direction a set of parallel rays are casted towards the objects as shown in Figure 6.(b) for a single direction. Each ray is associated with a value of optical depth, which is initialized to 0 and incremented for each voxel crossed by the ray by the amount $l\ d$, where l is the lenght of portion of ray inside the voxel and d is the density of the material associated with the voxel. At the end of this step we have,

for each voxel, its optical depth for each of the n directions.

Compute first moment of optical depth $\mathbf{T}(x)$
The first moment is easily computed for each voxel as the average of optical depth over all the n directions.

Compute divergence of first moment $\rho(x) = |\nabla \cdot \mathbf{T}(x)|$
The divergence is computed by finite difference operator over neighbors voxels (Figure 6.(c)).

Sampling the volume
After the estimation of the desired density we want to actually compute a set of N_s sample points whose density agree with $\rho(x)$ and that are spatially well distributed. Poisson Disks sampling [5] generates a set of points such that every point has a surrounding empty space of radius r (in other words there are not two points closer than r). One of the classical techniques for generating such distribution is the *dart throwing* approach, simple to be implemented but with the limitation that is difficult to get very closely packed Poisson Disk distributions. In particular we use a weighted Poisson Disk Sampling where the empty-space radius varies according to $\rho(x)$ as follows. Let r be a base radius computed as $\sqrt[3]{\frac{V}{2N_s}}$, assuming that we are not targeting a tight packing. We define $\delta = \frac{1}{2}r + \frac{3}{2}\frac{\rho_{max}-\rho_{min}}{\rho-\rho_{min}}r$, i.e. allow δ to vary between $\frac{r}{2}$ and $2r$. Then, the value of the ray for a given voxel is obtained by mapping the value $\frac{1}{\rho}$ between $\frac{r}{2}$ and $2*r$.

Compute SH
Finally, for each sample, the direction dependent optical depth is compressed by means of spherical harmonics.

5 Results and Discussion.

We implemented our algorithm in C++ and OpenGL, using OpenCL for the preprocessing phase and and GLSL for the shader programs in the rendering phase. All the tests were run on a Core 2 Duo @ 3.0 GHz 4GB RAM equipped with Nvidia GeForce 9800 GX2 512MB graphics card.

5.1 Comparison with ground truth

Our method relies on an approximation scheme configurable with a three parameters: the number of samples, the number of directions and the number of SPH coefficients. We do not give a formal proof of the bound on the error committed as a function of these parameters, but we can empirically show their influence by comparing images generated with our algorithm with the ground truth image obtained by ray tracing the original density field and integrating single scattering along the rays. Note that in this context "ground truth" is only referred to the single scattered contribution, which is the focus of this work, therefore the other phenomema are ignored in producing the image.

The first column of Table 1 shows the ground truth image for a view of a homogeneous sphere, while the next 3 columns show images taken with our method at an

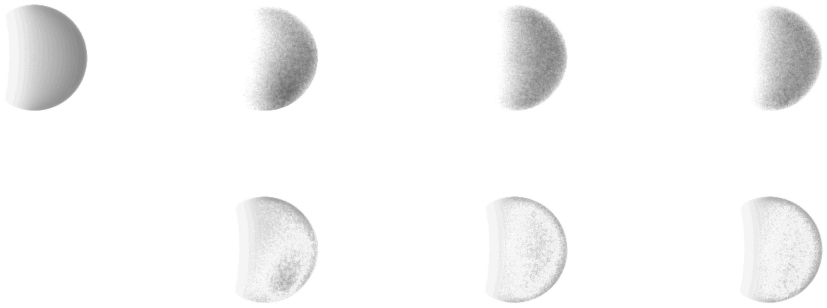

ground truth | 32 dir. 49395 samples | 128 dir. 53354 samples | 512 dir. 55237 samples

Table 1 Dependency of the approximation on the number of sampling directions. The top image is the ground truth, on the left column our approximationa and on the right the difference with the ground truth. Original pixels values are inverted compressed in a darker range to make the result visible when printing.

increasing number of sampling directions (upper row) and the pixel by pixel difference with the ground truth image (lower row). Note that the number of final sampling points increases with the number of directions. This is due to the fact that more directions capture more features and confirms that the divergence criterion adopted to sample the direction dependent optical depth is effective.

The Figure 7 shows two artificial examples. In the first example we place a torus inside a cube as shown in Figure 7.a and process the dataset considering the cube as the boundary of a translucent object containing an opaque part (the torus). Figure 7.b shows the result of our rendering algorithm putting behind the cube a single white light. Note that the geometric description of the torus is no more part of the dataset, but the sampling of the direction dependent optical depth captures its effect on the scattering of light inside the volume. A similar example is shown in Figure 7.c, where two lights (a white and a red one) are placed roughly symmetrically about the cube. Figure 7.d shows a dataset composed of a cube which volume is procedurally defined as a set of layers with two different density values, visible in the rendering. Figure8 shows few examples of rendering objects with our algorithm. In all cases

5.2 Efficiency

The preprocessing time of our algorithm is dominated by the time to compute the directional dependent depth opacity, which in turn is linearly proportional to the number of directions. Table 2 show the preprocessing times decomposed for the steps described in Section 4. The number of frames per time is linearly proportional to the number of samples used, and in all our experiments with a single light is constantly over 60 for a number of samples ranging from $8k$ to $11k$.

Table 3 shows that the fps decrease is only sub-linearly the increasing of the number of lights. This results is obtained because, thanks to the precomputation of the direction-dependent optical depth, adding a light only costs one more evaluation of the spherical harmonics. Table 4 shows the linear relation between rendering time and

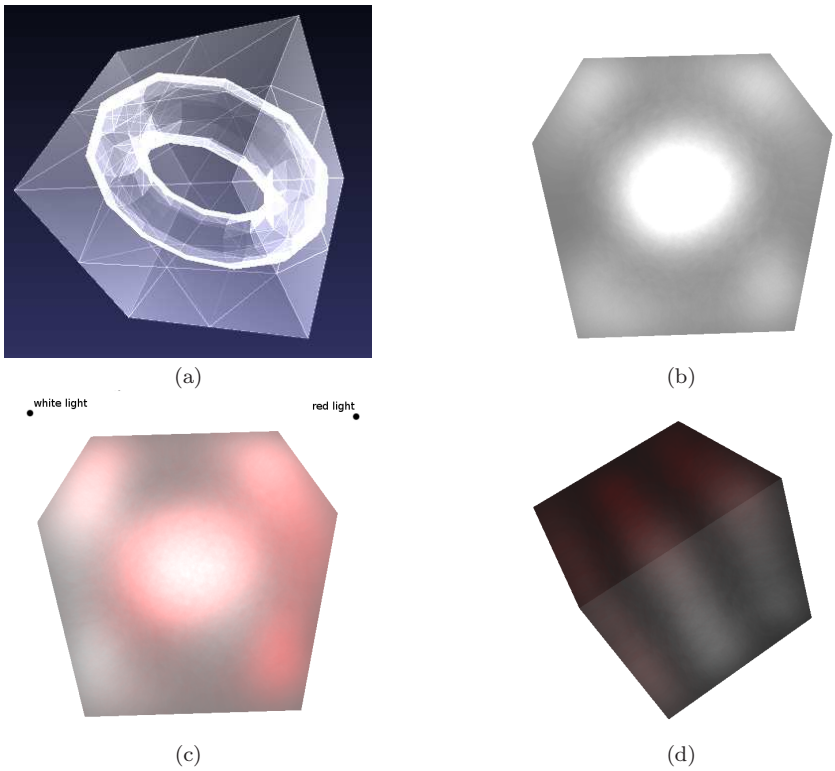

(a) (b) (c) (d)

Fig. 7 (a) a cube with a torus inside. The cube is taken as external boundary of a translucent object and the torus as an opaque blocker. (b-c) Two renderings that show how the effect of the blocker is captured by the sampling. (d) a procedural volume with two values of density arranges in parallel layers.

DDOD	Div	PDS	SPH coeff
43.02	1.76	15.39	28.92
168	1.71	17.64	112
664	1.78	19.16	446

Table 2 Construction times (in seconds) for the gargoyle model varying the number of directions for constructing the direction-dependent optical depth. DDOD: time for direction dependent optical depth computation; Div time for computing the divergence; PDS: time for the Poisson Disk Sampling algorithm; SPH: time for the spherical harmonic coefficients.

n. lights	2	4	7	8
fps	62	51	42	38

Table 3 FPS when augmenting the number of lights in a scene with 58297 samples with 25 SPH coefficients on a 800×800 viewport.

number of samples. It can be seen that the algorithm produces over 30 FPS with $100K$ samples.

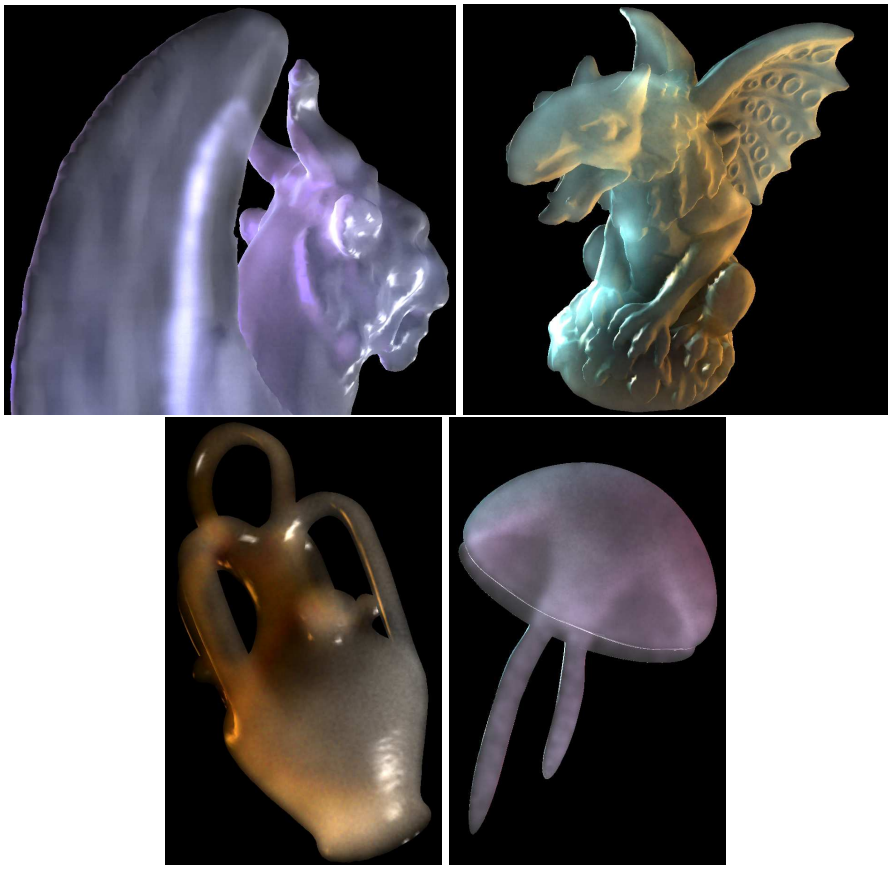

Fig. 8 Rendering of translucent objects: the feline statue (10321 samples), the gargolyle model (18385), the botjio (22722 samples) and a jellyfish (12227 samples), all rendered using 25 SPH coefficients. In all cases the FPS is constantly above 120.

n. samples	25000	50001	107833
fps	117	55	31

Table 4 FPS in relation to the number of sample on a 800×800 viewport.

5.3 Discussion

As in [36,37] our approach represents the volume with radial basis functions to compute scattering effects. The main difference is that in our algorithm the samples do not store density but a direction dependent optical depth. In this way the ray marching can be done without sorting the sphere front-to-back and so avoiding the overlinear cost of sorting algorithm and allowing us to use a much greater number of particles. As a consequence, we have a reduced approximation error which allows us to obtain satisfying visual results even without applying compensation for residual errors, and to sustain a higher fps. Clearly this is possible because the object is assumed to be static and the direction dependent optical depth does not changes over time.

6 Conclusions and future work

In this paper we have presented as real time rendering algorithm capable to reproduce single scattering inside inhomogeneous materials. We derived a formulation of the volume rendering equation in terms of a volumetric sampling of the direction-dependent optical depth, enabling the precomputation of the single scattering behavior as a function of incoming light. In addition, we exploited the behavior of such function to define a sound heuristic to define an adaptive sampling density and provided a efficient strategy to place the samples inside the model. Among the benefits of our approach, its running time shows little dependency on the number of lights and only a linear dependency on the number of samples used, since they do not need to be sorted at run time.

Since it requires a precomputation step, our approach cannot be used as it is for animate objects. However, we envision a future direction of work in supporting low degree deformations, which can be done by deriving local rigid transformations from the deformation and rotating the SPH of the samples accordingly.

The Fresnel deviation effects have not been entirely considered in this model. More precisely, the deviation of the rays of light penetrating the object can be easily considered during the construction, while the deviation of exiting rays is more complicated and it is matter of ongoing work. In order to use our model in a practical setting, we would also like to derive a multiresolution version, so that when it is far from the viewer, less samples and/or samples with smaller SPH are used.

Aknowledgements

The authors wish to thank Marco Di Benedetto from the Visual Computing Lab of ISTI-CNR for his precious GPU tips and tricks and Matteo Prayer-Galletti from the Universiá di Firenze for modeling the jellyfish shown in Figure 8. The research leading to these results has received funding from the EG 7FP IP “3D-COFORM” project (2008-2012, n. 231809) and from the Regione Toscana initiative “START”.

References

1. V. Biri, D. Arqués, and S. Michelin. Real time rendering of atmospheric scattering and volumetric shadows. In *Journal of WSCG'06*, pages 65–72. WSCG, 2006.
2. James F. Blinn. Light reflection functions for simulation of clouds and dusty surfaces. *SIGGRAPH Comput. Graph.*, 16(3):21–29, 1982.
3. Nathan A. Carr, Jesse D. Hall, and John C. Hart. GPU algorithms for radiosity and subsurface scattering. In *HWWS '03: Proceedings of the ACM SIGGRAPH/EUROGRAPHICS conference on Graphics hardware*, pages 51–59, Aire-la-Ville, Switzerland, Switzerland, 2003. Eurographics Association.
4. Eva Cerezo, Frederic Perez-Cazorla, Xavier Pueyo, Francisco Seron, and François Sillion. A Survey on Participating Media Rendering Techniques. *the Visual Computer*, 2005.
5. Robert L. Cook. Stochastic sampling in computer graphics. *ACM Trans. Graph.*, 5(1):51–72, 1986.
6. Carsten Dachsbacher and Marc Stamminger. Translucent shadow maps. In *EGRW '03: Proceedings of the 14th Eurographics workshop on Rendering*, pages 197–201, Aire-la-Ville, Switzerland, Switzerland, 2003. Eurographics Association.
7. Yoshinori Dobashi, Kazufumi Kaneda, Hideo Yamashita, Tsuyoshi Okita, and Tomoyuki Nishita. A Simple, Efficient Method for Realistic Animation of Clouds. In Kurt Akeley, editor, *Siggraph 2000, Computer Graphics Proceedings*, Annual Conference Series, pages 19–28. ACM Press / ACM SIGGRAPH / Addison Wesley Longman, 2000.

8. Robert Geist, Karl Rasche, James Westall, and Robert Schalkoff. Lattice-Boltzmann Lighting. In Alexander Keller and Henrik Wann Jensen, editors, *Eurographics Symposium on Rendering*, pages 355–362, Norrkoping, Sweden, 2004. Eurographics Association.
9. Pat Hanrahan and Wolfgang Krueger. Reflection from layered surfaces due to subsurface scattering. In *SIGGRAPH '93: Proceedings of the 20th annual conference on Computer graphics and interactive techniques*, pages 165–174, New York, NY, USA, 1993. ACM.
10. Xuejun Hao and Amitabh Varshney. Real-time rendering of translucent meshes. *ACM Trans. Graph.*, 23(2):120–142, 2004.
11. Mark J. Harris and Anselmo Lastra. Real-time cloud rendering. In *Computer Graphics Forum*, pages 76–84. Blackwell Publishing, 2001.
12. Kyle Hegeman, Michael Ashikhmin, and Simon Premože. A lighting model for general participating media. In *I3D '05: Proceedings of the 2005 symposium on Interactive 3D graphics and games*, pages 117–124, New York, NY, USA, 2005. ACM.
13. Wojciech Jarosz. Radiance caching for participating media. *ACM Transactions on Graphics*, 27(1):1, 2008.
14. Henrik Wann Jensen and Juan Buhler. A rapid hierarchical rendering technique for translucent materials. In *SIGGRAPH '02: Proceedings of the 29th annual conference on Computer graphics and interactive techniques*, pages 576–581, New York, NY, USA, 2002. ACM.
15. Henrik Wann Jensen and Per H. Christensen. Efficient simulation of light transport in scences with participating media using photon maps. In *SIGGRAPH '98: Proceedings of the 25th annual conference on Computer graphics and interactive techniques*, pages 311–320, New York, NY, USA, 1998. ACM.
16. Henrik Wann Jensen, Stephen R. Marschner, Marc Levoy, and Pat Hanrahan. A practical model for subsurface light transport. In *SIGGRAPH '01: Proceedings of the 28th annual conference on Computer graphics and interactive techniques*, pages 511–518, New York, NY, USA, 2001. ACM.
17. Juan-Roberto Jimènez, Karol Myszkowski, and Xavier Pueyo. Interactive global illumination in dynamic participating media using selective photon tracing. In *SCCG '05: Proceedings of the 21st spring conference on Computer graphics*, pages 211–218, New York, NY, USA, 2005. ACM.
18. James T. Kajiya and Brian P. Von Herzen. Ray Tracing Volume Densities. In *Computer Graphics (ACM SIGGRAPH '84 Proceedings)*, volume 18, pages 165–174, jul 1984.
19. Joe Kniss, Simon Premoze, Charles Hansen, and David Ebert. Interactive Translucent Volume Rendering and Procedural Modeling. *Visualization Conference, IEEE*, 0, 2002.
20. Joe Kniss, Simon Premoze, Charles Hansen, Peter Shirley, and Allen McPherson. A Model for Volume Lighting and Modeling. *IEEE Transactions on Visualization and Computer Graphics*, 9(2):150–162, 2003.
21. Eric P. Lafortune and Yves D. Willems. Rendering Participating Media with Bidirectional Path Tracing. In Xavier Pueyo and Peter Schröder, editors, *Rendering Techniques '96*, Eurographics, pages 91–100. Springer-Verlag Wien New York, 1996.
22. Tom Mertens. Efficient Rendering of Local Subsurface Scattering. *Computer Graphics Forum*, 24(1):41, 2005.
23. Tom Mertens, Jan Kautz, Philippe Bekaert, Hans-Peter Seidelz, and Frank Van Reeth. Interactive rendering of translucent deformable objects. In *EGRW '03: Proceedings of the 14th Eurographics workshop on Rendering*, pages 130–140, Aire-la-Ville, Switzerland, Switzerland, 2003. Eurographics Association.
24. Srinivasa G. Narasimhan and Shree K. Nayar. Shedding light on the weather. In *In CVPR 03*, pages 665–672, 2003.
25. Simon Premože, Michael Ashikhmin, and Peter Shirley. Path Integration for Light Transport in Volumes. Eurographics Symposium on Rendering 2003, pp. 1-12 Per Christensen and Daniel Cohen-Or (Editors) , 2003.
26. Holly Rushmeier. *Realistic Image Synthesis for Scenes with Radiatively Participating Media*. PhD thesis, Cornell University, 1988.
27. Holly E. Rushmeier and Kenneth E. Torrance. The Zonal Method for Calculating Light Intensities in the Presence of a Participating Medium. In *Computer Graphics (ACM SIGGRAPH '87 Proceedings)*, volume 21, pages 293–302, jul 1987.
28. Peter-Pike Sloan, Jesse Hall, John Hart, and John Snyder. Clustered principal components for precomputed radiance transfer. *ACM Trans. Graph.*, 22(3):382–391, 2003.

29. Peter-Pike Sloan, Jan Kautz, and John Snyder. Precomputed radiance transfer for real-time rendering in dynamic, low-frequency lighting environments. In *SIGGRAPH '02: Proceedings of the 29th annual conference on Computer graphics and interactive techniques*, pages 527–536, New York, NY, USA, 2002. ACM.
30. Jos Stam. Stochastic rendering of density fields. In *Graphics Interface '94*, pages 51–58, may 1994.
31. Jos Stam. Multiple scattering as a diffusion process. In *In Eurographics Rendering Workshop*, pages 41–50, 1995.
32. Bo Sun, Ravi Ramamoorthi, Srinivasa G. Narasimhan, and Shree K. Nayar. A practical analytic single scattering model for real time rendering. *ACM Trans. Graph.*, 24(3):1040–1049, 2005.
33. Bruce Walter, Shuang Zhao, Nicolas Holzschuch, and Kavita Bala. Single scattering in refractive media with triangle mesh boundaries. *ACM Transactions on Graphics*, 28(3), aug 2009.
34. Rui Wang, John Tran, and David Luebke. All-frequency interactive relighting of translucent objects with single and multiple scattering. In *SIGGRAPH '05: ACM SIGGRAPH 2005 Papers*, pages 1202–1207, New York, NY, USA, 2005. ACM.
35. Yajun Wang, Jiaping Wang, Nicolas Holzschuch, Kartic Subr, Jun-Hai Yong, and Baining Guo. Real-time Rendering of Heterogeneous Translucent Objects with Arbitrary Shapes. *Computer Graphics Forum*, 29, 2010. I.: Computing Methodologies/I.3: COMPUTER GRAPHICS/I.3.7: Three-Dimensional Graphics and Realism.
36. Kun Zhou. Real-time smoke rendering using compensated ray marching. *ACM Transactions on Graphics*, 27(3):1, 2008.
37. Kun Zhou, Qiming Hou, Minmin Gong, John Snyder, Baining Guo, and Heung-Yeung Shum. Fogshop: Real-Time Design and Rendering of Inhomogeneous, Single-Scattering Media. In *PG '07: Proceedings of the 15th Pacific Conference on Computer Graphics and Applications*, pages 116–125, Washington, DC, USA, 2007. IEEE Computer Society.